Journal of Materials Chemistry C

Accepted Manuscript

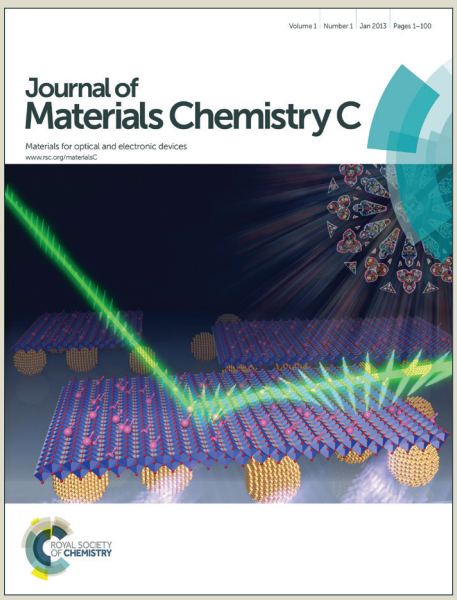

ROYAL SOCIETY OF CHEMISTRY

www.rsc.org/materialsC

Journal Name

RSCPublishing

ARTICLE

An Efficient Light Converter YAB: Cr^{3+}, Yb^{3+}/Nd^{3+} with Broadband Excitation and Strong NIR emission for Harvesting c-Si-based Solar Cell

Cite this: DOI: 10.1039/x0xx00000x

Received ooth January 2012,
Accepted ooth January 2012

DOI: 10.1039/x0xx00000x

www.rsc.org/

Pujun Liu[a], Jie Liu[a]*, Xiao Zheng[a], Hongde Luo[a], Xiaoqing Li[a], Zhiling Yao[a], Xibin Yu[a]*, Xiumeng Shi[b], Binghu Hou[a], Yusheng Xia[a]

Highly efficient Cr^{3+}- and Yb^{3+}/Nd^{3+} -co-activated $YAl_3(BO_3)_4$ (YAB) phosphors have been developed as spectral convertors for improving silicon solar cell photovoltaic conversion efficiency. In the YAB lattice, Cr^{3+} ions act as broadband spectral sensitizers by absorbing UV-Vis (370–750 nm) photons, which are not absorbed by silicon solar cell. After energy transfer, the Yb^{3+} acceptors then exhibit strong NIR emission centered at around 1000 nm, which is coupled well with the absorption band of the silicon solar cell. Efficient energy transfer is reflected by a sharp decrease in the excited state lifetime and red photoluminescence (PL) from Cr^{3+} with increasing Yb^{3+} concentration. Another evidence in favor of energy transfer is that PL-excitation spectra of NIR luminescence from Yb^{3+} are identical to those of deep red emission from Cr^{3+}. Trivalent ions Gd^{3+}, Bi^{3+} and La^{3+} have been introduced into $YAl_3(BO_3)_4$:Cr^{3+},Yb^{3+} in this study for stronger NIR PL intensity. Additionally, energy transfer from Cr^{3+} to Nd^{3+} is also observed. Yb^{3+}, Nd^{3+} -co-activated YAB shows much broader NIR emission. Due to the effective absorption of Cr^{3+} in the visible region in YAB and the efficient energy transfer to Yb^{3+}/Nd^{3+}, these materials can be developed as spectral convertors to improve silicon solar cell photovoltaic conversion efficiency.

1. Introduction

Sunlight is a free, green and abundant source of energy that can be captured by photovoltaic cells and transformed into electricity.[1, 2] If the tiniest fraction of that sunlight were to be captured by photovoltaic cells that turn it straight into electricity, there would be no need to emit any greenhouse gases from any power plant.[3] Despite significant development of the photovoltaic (PV) industry over the past decades, the efficient conversion of solar energy into electricity through PV cells remains a daunting task.[4] The main source of energy loss (over 70%) is related to the spectral mismatch of incident solar photon energies to the energy gap (E_g) of a solar cell.[5, 6] Solar cells generate a single electron–hole pair upon absorbing a photon above the band gap, means that photons with energy higher than the band gap are absorbed, but the excess energy is not effectively used and released as heat.[1]

The rare earth (RE) ions doped luminescent materials can convert the near-UV and visible absorption into near-infrared emission around 1000 nm have attracted intensive interests due to their promising application as spectral convertors to improve the photovoltaic conversion of c-Si solar cells. Among these researches, the Yb^{3+} ion has been identified as an almost ideal acceptor species for this purpose, as it possesses only a single excited state,$^2F_{2/5}$, which is located close to the maximum of the spectral efficiency of c-Si solar cells.[6, 7] Various trivalent RE ions, such as Pr^{3+}, Ho^{3+}, Er^{3+}, Tb^{3+} and Tm^{3+}, were firstly selected as the energy sensitizers for Yb^{3+} ions to realize the spectral conversion.[6, 8-12] However, only a small portion of the sunlight can be converted in these systems due to the nature of f-f transition. In order to take better use the incident sunlight, the RE ions with f-d transition, such as such as Ce^{3+}, Eu^{2+} and Yb^{2+},[12-14] the mental ions, such as Bi^{3+},[15] were chosen as the energy donors for Yb^{3+} to realize the broadband spectral conversion.

The Cr^{3+} also has broad absorption bands in the visible region due to the spin allowed $^4A_2 \rightarrow {}^4T_2$ and $^4A_2 \rightarrow {}^4T_1$ transitions, thus has been widely used as a luminescent sensitizer for RE ions, to obtain high excitation efficiency.[16] For practical application, the spectral convertors need to be effectively activated by natural sunlight and also should be stable enough to survive the outside atmosphere. In this case, the selection of proper energy absorbers with high pump efficiency and broadband absorption, and the choosing of environmental friendly hosts with excellent chemical, mechanical and thermal stabilities are of great importance.

On the other side, the yttrium aluminum borate $YAl_3(BO_3)_4$ (YAB) is one of the most desirable hosts for RE ions. One good example that combined the merits of Cr^{3+} broadband absorption and YAB excellent chemical and mechanical stability is the Cr^{3+}-Doped YAB Single Crystals. Due to the high efficient absorption of Cr^{3+} ions in the YAB host, this material has been suggested to be used in

the solar-pumped lasers, in which the solar radiation was used as the pumping source.[17, 18]

In this work we have studied the optical spectroscopy of Cr^{3+}-Yb^{3+}, Cr^{3+}-Nd^{3+} and Cr^{3+}-Yb^{3+}-Nd^{3+}-doped YAB crystals. In our research, the YAB was chosen as the doping host for Cr^{3+} and Yb^{3+}, in which the Cr^{3+} acts as the energy absorber to harvest the incident sunlight and meanwhile the energy sensitizer for Yb^{3+}/Nd^{3+}. Trivalent ions Gd^{3+}, Bi^{3+} and La^{3+} had been introduced into YAB: Cr^{3+}, Yb^{3+} in this study for stronger NIR PL intensity, and Nd^{3+} for broader NIR PL bandwidth. By taking advantage of the spin allowed $^4A_2 \rightarrow {}^4T_2$ and $^4A_2 \rightarrow {}^4T_1$ absorption of Cr^{3+} and the efficient energy transfer to Yb^{3+}. The outstanding point of Cr^{3+}-Yb^{3+} co-doped YAB compared with other phosphors is that YAB: Cr^{3+}, Yb^{3+} can convert almost high-energy UV-Vis photons into low-energy NIR photons efficiently, which benefit the enhancement of silicon solar photovoltaic conversion efficiency.

2. Experimental Section

Synthesis. The powder samples of $YAl_3(BO_3)_4$ phosphors were prepared by a conventional solid-state reaction. The starting materials Y_2O_3 99.9%, Al_2O_3 99.9%, Cr_2O_3 99.9%, Yb_2O_3 99.9%, Nd_2O_3 99.9%, Lu_2O_3 99.9%, Gd_2O_3 99.9%, Bi_2O_3 99.9%, La_2O_3 99.9% were weighed in stoichiometric amounts (excess amount of H_3BO_3 99.9% were added to obtain a single phase) and subsequently mixed and ground together by grinding in an agate mortar. The powder mixtures were synthesized by sintering at 1200 °C for 5h. The as-synthesized samples were then cooled to room temperature naturally. Finally, the samples were ground into powder for subsequent analysis.

Characterization. All measurements were made on finely ground powder. The structure of as-prepared samples was checked by a Rigaku DMAX 2000 diffractometer equipped with Cu Kα radiation (λ=0.15405nm) (40kV, 40mA). Rietveld refinements of the X-ray diffractograms were conducted using the MAUD (Materials Analysis Using Diffraction) program. And the photoluminescence excitation (PLE) spectra, the photoluminescence (PL) spectra and the luminescence decay in visible and infrared regions were recorded by using a FLS920 fluorescence spectrophotometer. The absorption spectra were recorded with Cary 500 UV-vis-NIR spectrophotometer by using $BaSO_4$ as a reference. An electrochemical workstation (ZAHNER Zennium, Germany) was used to obtain the current–voltage characteristics of the commercial c-Si solar cells before and after employing the luminescent down-shifting phosphor YAB:Cr^{3+},Yb^{3+}. The total cell area measured is 9 cm^2. The illumination of AM1.5G simulated solar light during the measurements coming from an Oriel Sol 3A solar simulator (Newport-69920) equipped with a Xe lamp (450 W) and an AM1.5G filter. EQE is measured by a measured by controlled intensity modulated photospectroscopy (CIMPS-2, Zahner Co., Germany) in ambient conditions.

3. Results and Discussion

3.1 XRD Refinement and Lattice Parameters.

The phase purities of the $YAl_{2.79}Cr_{0.21}(BO_3)_4$, $Y_{0.93}Yb_{0.07}Al_{2.79}Cr_{0.21}(BO_3)_4$ and $Y_{0.88}Yb_{0.07}Bi_{0.05}Al_{2.79}Cr_{0.21}(BO_3)_4$ compounds were confirmed using X-ray powder diffraction (XRD). The Rietveld refinements from XRD patterns indicate that these three compounds exhibit the same crystalline trigonal crystal system. Additionally, the Rietveld refinement results demonstrate that the as-prepared phosphors were $YAl_3(BO_3)_4$ (JCPDS Card No.72-1978), typically one impurity phase $Al_{20}B_4O_{36}$ (JCPDF Card No.80-2300) were identified (Figure 1). Huntite-type $YAl_3(BO_3)_4$ belongs to the space group R32 with cell parameters of a = b = 9.295Å, c = 7.243Å, α = β = 90° and γ=120 °. The concentration of the impurity phases $Al_{20}B_4O_{36}$ in $YAl_{2.79}Cr_{0.21}(BO_3)_4$, $Y_{0.93}Yb_{0.07}Al_{2.79}Cr_{0.21}(BO_3)_4$ and $Y_{0.88}Yb_{0.07}Bi_{0.05}Al_{2.79}Cr_{0.21}(BO_3)_4$ were 2.29%,3.47%,4.93% wt %,respectively. Notably, a small quantity of impurity phases negligibly affects the energy transfer.[19-21] The detailed crystallographic data are listed in Table 1. Fractional coordinates of $YAl_{2.79}Cr_{0.21}(BO_3)_4$, $Y_{0.93}Yb_{0.07}Al_{2.79}Cr_{0.21}(BO_3)_4$, and $Y_{0.88}Yb_{0.07}Bi_{0.05}$ $Al_{2.79}Cr_{0.21}(BO_3)_4$ are shown in Table 2. The crystal structures of $YAl_{2.79}Cr_{0.21}(BO_3)_4$, $Y_{0.93}Yb_{0.07}Al_{2.79}Cr_{0.21}(BO_3)_4$ and $Y_{0.88}Yb_{0.07}Bi_{0.05}Al_{2.79}Cr_{0.21}(BO_3)_4$ from the literature were used as the initial parameters for the Rietveld refinement of the prepared powders. Figure 1 presents the results of the experimental and the calculated X-ray powder diffraction patterns for $YAl_{2.79}Cr_{0.21}(BO_3)_4$, $Y_{0.93}Yb_{0.07}Al_{2.79}Cr_{0.21}(BO_3)_4$ and $Y_{0.88}Yb_{0.07}Bi_{0.05}Al_{2.79}Cr_{0.21}(BO_3)_4$, and the corresponding residuals using the Rietveld refinement.

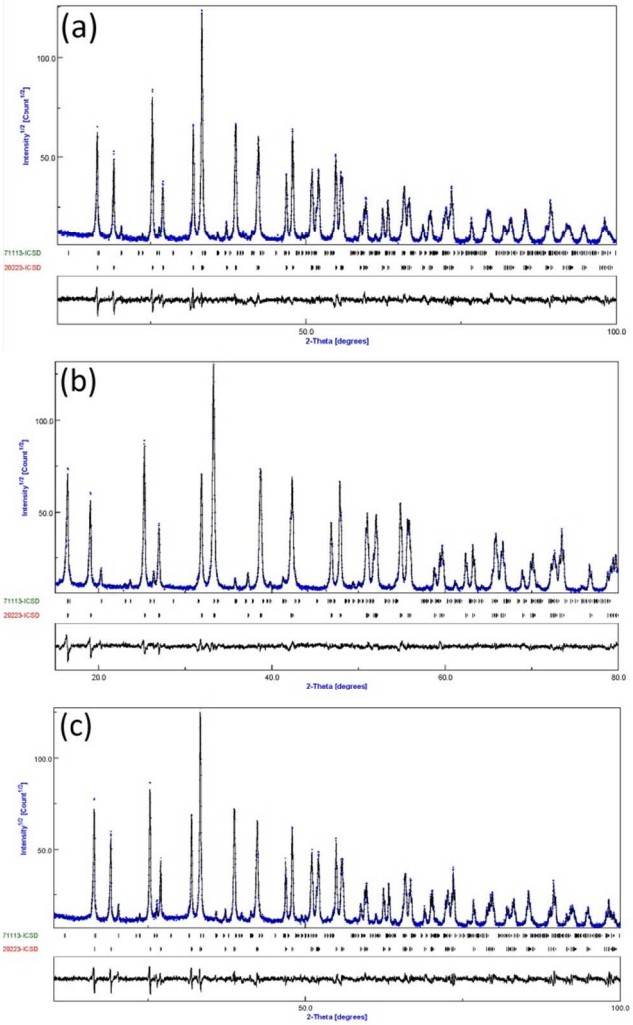

Figure 1. Powder X-ray diffraction spectra refinement of (a)

$YAl_{2.79}Cr_{0.21}(BO_3)_4$, (b) $Y_{0.93}Yb_{0.07}Al_{2.79}Cr_{0.21}(BO_3)_4$, and (c) $Y_{0.88}Yb_{0.07}Bi_{0.05}Al_{2.79}Cr_{0.21}(BO_3)_4$. Blue crosses are observed and the black lines are calculated.

Table 1. Crystallographic Data for (a) $YAl_{2.79}Cr_{0.21}(BO_3)_4$, (b) $Y_{0.93}Yb_{0.07}Al_{2.79}Cr_{0.21}(BO_3)_4$, and (c) $Y_{0.88}Yb_{0.07}Bi_{0.05}Al_{2.79}Cr_{0.21}(BO_3)_4$ As Determined from Rietveld Refinement

Formula	$YAl_{2.79}Cr_{0.21}(BO_3)_4$	$Y_{0.93}Yb_{0.07}Al_{2.79}Cr_{0.21}(BO_3)_4$	$Y_{0.88}Yb_{0.07}Bi_{0.05}Al_{2.79}Cr_{0.21}(BO_3)_4$
Crystal System	Trigonal	Trigonal	Trigonal
Space Group	R32	R32	R32
a (Å)	9.2845(1)	9.2843(2)	9.2807(1)
b (Å)	9.2845(1)	9.2843(2)	9.2807(1)
c (Å)	7.2392(1)	7.2330(1)	7.2287(2)
α (deg)	90	90	90
β (deg)	90	90	90
λ (deg)	120	120	120
V (Å^3)	540.428	539.91	539.20
R_{wp} (%)	8.57	7.62	9.75
R_{exp} (%)	5.91	5.31	6.28

Table 2. Fractional coordinates from the Rietveld refinement of (a) $YAl_{2.79}Cr_{0.21}(BO_3)_4$, (b) $Y_{0.93}Yb_{0.07}Al_{2.79}Cr_{0.21}(BO_3)_4$, and (c) $Y_{0.88}Yb_{0.07}Bi_{0.05}Al_{2.79}Cr_{0.21}(BO_3)_4$

	$YAl_{2.79}Cr_{0.21}(BO_3)_4$					
Atom	Site	x	y	z	Occupancy	U_{iso}
Al	9d	0.5563	0	0	0.93	0.17
Cr	9d	0.5563	0	0	0.07	0.17
B1	3b	0	0	0.5	1	0.41
B2	9e	0.4476	0	0.5	1	0.36
O1	9e	0.8520	0	0.5	1	0.31
O2	9e	0.5914	0	0.5	1	0.37
O3	18f	0.4507	0.1532	0.5011	1	0.44
Y	3a	0	0	0	1	0.63

	$Y_{0.93}Yb_{0.07}Al_{2.79}Cr_{0.21}(BO_3)_4$					
Atom	site	x	y	z	Occupancy	U_{iso}
Al	9d	0.5571	0	0	0.93	0.19
Cr	9d	0.5571	0	0	0.07	0.19
B1	3b	0	0	0.5	1	0.40
B2	9e	0.4543	0	0.5	1	0.33
O1	9e	0.8491	0	0.5	1	0.39
O2	9e	0.5919	0	0.5	1	0.48
O3	18f	0.4502	0.1537	0.5036	1	0.46
Y	3a	0	0	0	0.93	0.67
Yb	3a	0	0	0	0.07	0.67

	$Y_{0.88}Yb_{0.07}Bi_{0.05}Al_{2.79}Cr_{0.21}(BO_3)_4$					
Atom	site	x	y	z	Occupancy	U_{iso}
Al	9d	0.5557	0	0	0.93	0.22
Cr	9d	0.5557	0	0	0.07	0.22
B1	3b	0	0	0.5	1	0.42
B2	9e	0.4494	0	0.5	1	0.36
O1	9e	0.8543	0	0.5	1	0.41
O2	9e	0.5933	0	0.5	1	0.55
O3	18f	0.4497	0.1506	0.4986	1	0.47
Y	3a	0	0	0	0.88	0.69
Yb	3a	0	0	0	0.07	0.69
Bi	3a	0	0	0	0.05	0.69

Wang et al.[22] proposed both trivalent rare-earth and transition metal ions (e.g. Cr^{3+}) can be doped into the material, where rare-earth ions then occupy yttrium sites and transition metal ions replace Al^{3+} on sites of octahedral symmetry. Unquestionable trivalent rare-earth occupies yttrium sites.[17, 23] While they did not give any reliable evidence for the occupancy of Cr^{3+}.[17, 22, 24]

Table 3. Refinement results of different Cr^{3+} structure models in different sample

Formula	$YAl_{2.79}Cr_{0.21}(BO_3)_4$	$Y_{0.93}Yb_{0.07}Al_{2.79}Cr_{0.21}(BO_3)_4$	$Y_{0.88}Yb_{0.07}Bi_{0.05}Al_{2.79}Cr_{0.21}(BO_3)_4$
a (Å)	9.2845(1)	9.2843(2)	9.2807(1)
b (Å)	9.2845(1)	9.2843(2)	9.2807(1)
c (Å)	7.2392(1)	7.2330(1)	7.2287(2)
R_{wp} (%) (Al)	8.57	7.62	9.75
R_{wp} (%) (Y)	12.57	11.47	13.85

As an illustration, we tried to prepare two different Cr^{3+} doped YAB samples, Cr^{3+} ions occupy Al^{3+} site and Y^{3+} site, respectively. Results from experiments show that Cr^{3+} occupy Y^{3+} site samples presented more impurity phases than samples Cr^{3+} occupy Al^{3+}. This may preliminarily indicated that Cr^{3+} occupy the Al^{3+} site. More conclusive evidences was given in the results of the refinement, cell parameters of YAB with substitution of Al^{3+} by Cr^{3+} did not increase but slightly decrease. Repetitive experiments show the same results and only substitution of Al^{3+} by Cr^{3+} can get better results of Rietveld refinement (see in Table 3). It gives an explanation to the slight decrease in YAB lattice.

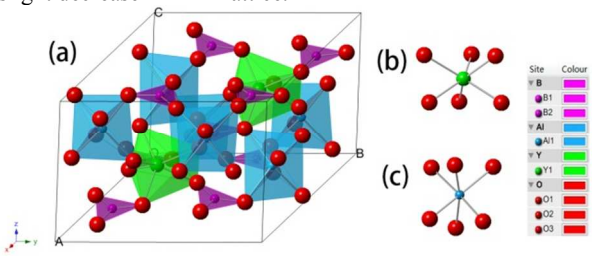

Figure 2. Unit cell representation of $Y_{0.88}Yb_{0.07}Bi_{0.05}Al_{2.79}Cr_{0.21}(BO_3)_4$ (a) and coordination environment of Y(b) and Al(c). Purple, blue, green and red spheres represent B, Al-Cr, Y-Yb-Bi and O atoms, respectively.

Figure 2 displays the unit cell representation of $Y_{0.88}Yb_{0.07}Bi_{0.05}Al_{2.79}Cr_{0.21}(BO_3)_4$. The 3a site in this structure is occupied by Yb^{3+}, Nd^{3+}, Gd^{3+}, Bi^{3+} and La^{3+} and the 9d site is occupied by Cr^{3+}.

3.2 Typical features of YAB:Cr^{3+},Yb^{3+}

To illustrate the advantage of our YAB:Cr^{3+},Yb^{3+}, we demonstrate the characterize the absorption spectra for the Cr^{3+}/Yb^{3+} -activated YAB (shown in Figure 3a). Purely YAB and YAB:Yb^{3+} nearly show none absorption in UV-Vis region. While YAB:Cr^{3+} shows wide absorption band from 370 to 750nm, composes of two broad bands centered around 425 and 590 nm, which correspond to the spin-

allowed (ΔS=0) $^4A_2 \rightarrow {}^4T_1$ and $^4A_2 \rightarrow {}^4T_2$ transitions, respectively. The small pumps at 683nm can be assigned to the spin-forbidden (ΔS=1) Cr^{3+} : $^4A_2 \rightarrow {}^2T_1$ absorption in a slightly distorted octahedral site.[25] The inset shows apparent color of $Y_{0.93}Yb_{0.07}Al_{2.71}Cr_{0.21}(BO_3)_4$. As we known the c-Si based cell can't make good use of the UV-Vis light, the broadband absorption bandwidth of YAB:Cr^{3+} is fabulous for efficient capture of the incident solar energy.

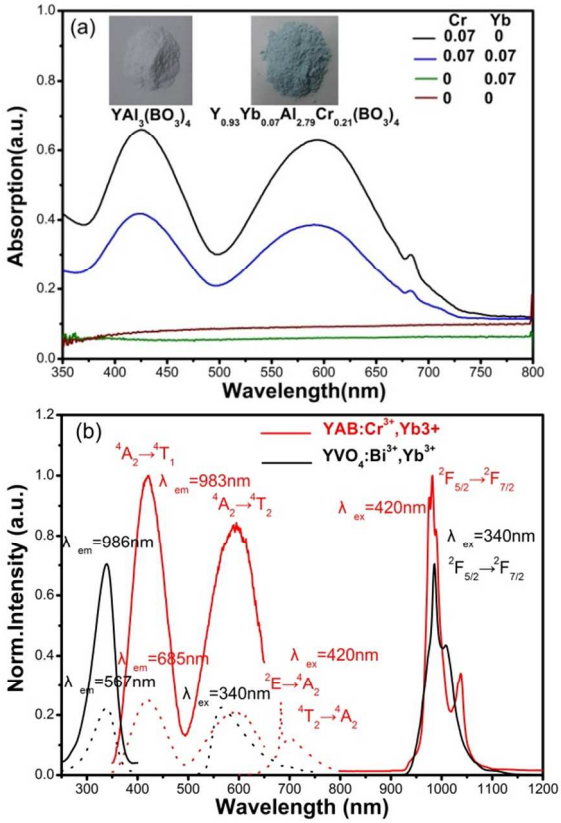

Figure 3.(a) Absorption spectra for different doped content, the inset circle is the apparent color of YAl_3 $(BO_3)_4$ and $Y_{0.93}Yb_{0.07}Al_{2.71}Cr_{0.21}(BO_3)_4$. (b) PLE and PL spectra of $Y_{0.93}Yb_{0.07}Al_{2.71}Cr_{0.21}(BO_3)_4$ (red line) and YVO_4:Bi^{3+},Yb^{3+} (black line), dash line monitored each visible part .

Thus we introduced Yb^{3+} to YAB:Cr^{3+} for converting UV-Vis sunlight to intense NIR emission. As shown in Figure 3b, YVO_4: Bi^{3+},Yb^{3+} was the best sample we prepared before.[7] Under the excitation of $^4T_1$ and $^4T_2$ energy levels at 425 and 590 nm, the PL spectra of Cr^{3+} were recorded (red dash line), the sharp R-line emission at 683 nm assigned to Cr^{3+} $^2E \rightarrow {}^4A_2$ transition, and a broadband emission located around 705 nm due to the spin allowed $^4T_2 \rightarrow {}^4A_2$ emission can be observed. The near-infrared emission at 983nm originated from Yb^{3+}: $^2F_{5/2} \rightarrow {}^2F_{7/2}$ transition can also be clearly observed under the excitations of Cr^{3+}:$^4T_1$ and $^4T_2$ energy levels, which wouldn't show in YAB:Yb^{3+}. It exhibits nearly the same PLE peak shape when monitored at 983nm (black solid line) and 683nm (red dash line), two intense broad bands centered at 425 and 590nm attributed to the typical spin-allowed $^4A_2 \rightarrow {}^4T_1$ and $^4A_2 \rightarrow {}^4T_2$ transitions of Cr^{3+}, also the same shape to the absorption spectra of YAB:Cr^{3+},Yb^{3+}, indicates the absorbed sunlight can be utilized, and the energy transfer from $Cr^{3+} \rightarrow Yb^{3+}$. Accordingly, we illustrate the simplified energy level diagrams of Cr^{3+} and Yb^{3+} in the YAB hosts (Figure 3c). We compared our best sample $Y_{0.93}Yb_{0.07}Al_{2.71}Cr_{0.21}(BO_3)_4$ with the well-known spectra convert phosphor YVO_4: Bi^{3+},Yb^{3+},[26, 27] it's obvious that the excitation band of $Y_{0.93}Yb_{0.07}Al_{2.71}Cr_{0.21}(BO_3)_4$ is broader than YVO_4: Bi^{3+},Yb^{3+}, and the NIR emission intensity of $Y_{0.93}Yb_{0.07}Al_{2.71}Cr_{0.21}(BO_3)_4$ is stronger than YVO_4: Bi^{3+},Yb^{3+}.

3.3 Optical Properties of $Y_{1-n}Yb_nAl_{2.79}Cr_{0.21}(BO_3)_4$ (n=0, 0.01, 0.03, 0.07, 0.11, 0.15)

This section describes the synthesis of the Cr^{3+}–Yb^{3+} system with a donor having a broad band excitation to verify its feasibility. The concentration of the activator is kept at 7% for Cr^{3+},[22] and that of Yb^{3+} concentration is changed from 0 to 15%.

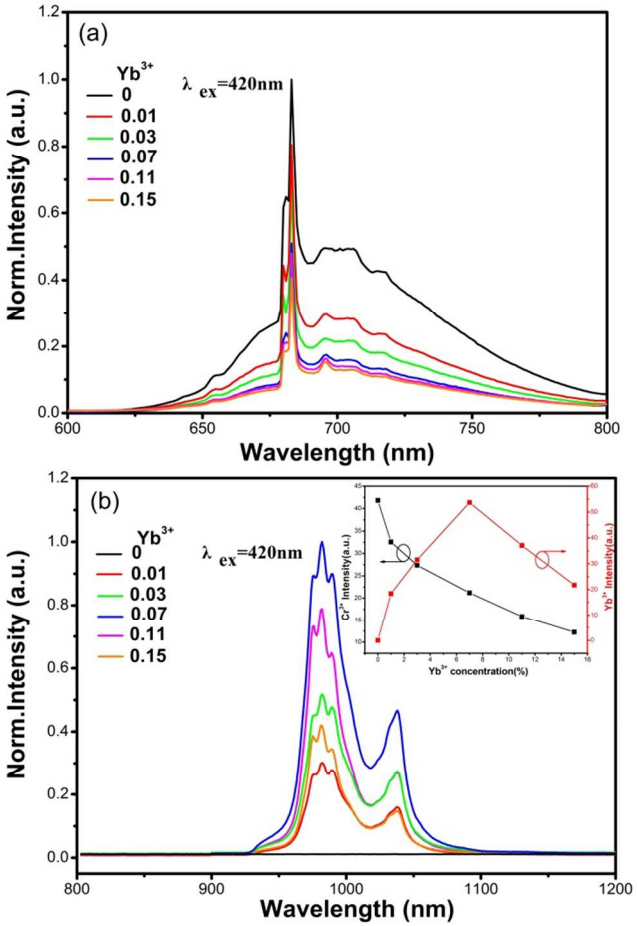

Figure 4. (a) Normalized emission spectra of $Y_{1-n}Yb_nAl_{2.71}Cr_{0.21}(BO_3)_4$ at the Vis region. (b) Normalized emission spectra of $Y_{1-n}Yb_nAl_{2.71}Cr_{0.21}(BO_3)_4$ at the NIR region, the inset shows the linear fitting of the degree in which Cr^{3+} decreases and Yb^{3+} changes.

Figure 4a shows the normalized Vis PL spectra for six Cr^{3+} and Yb^{3+} -co-activated $Y_{1-n}Yb_nAl_{2.71}Cr_{0.21}(BO_3)_4$ phosphors with different dopant contents n of 0, 0.01, 0.03, 0.07, 0.11, and 0.15, respectively. Under 420 nm excitation, the Vis PL intensity decreased with increasing concentration of Yb^{3+}. Figure 4b plots the NIR emission spectra of the samples with different Yb^{3+} concentration. As expected, no NIR PL is found in the studied spectral region from $Y_{1-n}Yb_nAl_{2.71}Cr_{0.21}(BO_3)_4$ (n=0). Only after co-doping with Yb^{3+}, a sharp peak with a maximum at 983 nm arises. This emission can be excited via the entire UV-Vis band from 370-650nm (date not

shown). All observed NIR emissions are readily attributed to radiative decay from the lowest stark level of Yb^{3+},$^2F_{2/5}$, to stark level of the ground state of Yb^{3+},$^2F_{2/7}$. The appearance of the characteristic NIR PL from Yb^{3+} centers is taken as a direct evidence for the energy transfer from Cr^{3+} to Yb^{3+}. In this case, Cr^{3+} acts as a sensitizer by absorbing UV-Vis photons and transferring the absorbed energy to Yb^{3+} centers. With increasing Yb^{3+} concentration, the emission intensity of Yb^{3+} increases, maximizing at about n=0.07, it also happened when excited at 590nm. Concentration quenching occurs, when n>0.07 (the inset of Figure4b). Concentration quenching is mainly caused by the non radiative energy transfer among Yb^{3+}, which usually occurs as a result of an exchange interaction, radiation reabsorption or a multipole-multipole.[28, 29]

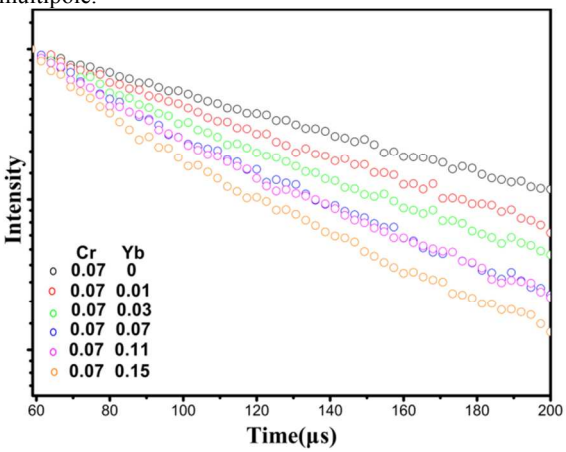

Figure 5. Photoluminescence decay curve of Cr^{3+} in $Y_{1-n}Yb_n(Al_{0.93}Cr_{0.07})_3(BO_3)_4$.

Normalized PL decay curves of Cr^{3+} in $Y_{1-n}Yb_nAl_{2.79}Cr_{0.21}(BO_3)_4$ were measured and are represented in Figure 5.As described by Blasse and Grabmaier,[30] it is well established that the decay behavior of Cr^{3+} can be expressed by

$$I=I_0\exp(-t/\tau) \quad (1)$$

, where I and I_0 are the luminescence intensities at time t and 0, and τ is the luminescence lifetime. On the basis of eq 1 and decay curves, the lifetime values were determined to be 158.39, 125.49, 104.35, 76.94, 68.79,and 60.52μs for $Y_{1-n}Yb_nAl_{2.79}Cr_{0.21}(BO_3)_4$ with n = 0, 0.01, 0.03, 0.07, 0.11, and 0.15, respectively. The decay lifetime for Cr^{3+} was found to decrease with increasing Yb^{3+} dopant content, which is strong evidence for the energy transfer from $Cr^{3+}\rightarrow Yb^{3+}$. According to Dexter and Schulman, concentration quenching is in many cases due to energy transfer from one activator to another until an energy sink in the lattice is reached.[22] As suggested by Blasse,[30] the average separation R_C can be expressed by

$$R_C=2\left[\frac{3V}{4\pi xN}\right]^{1/3} \quad (2)$$

where N is the number of Z ions in the unit cell, and V is the volume of the unit cell. For $YAl_3(BO_3)_4$ host, N=6 and V=540.4 Å^3. x is the total concentration of Cr^{3+} and Yb^{3+}. Thus, R_C (in Å) is determined to be 25.8, 17.9,13.5, 11.6, and 10.5 for n=0.01, 0.03, 0.07,0.11, and 0.15,respectively, in $Y_{1-n}Yb_nAl_{2-79}Cr_{0.21}(BO_3)_4$. The critical concentration x_c, at which the luminescence intensity of Cr^{3+} is half that in the sample in the absence of Yb^{3+}, is 0.07. Therefore, the critical distance (R_c) of energy transfer was calculated to be about 11.6 Å.

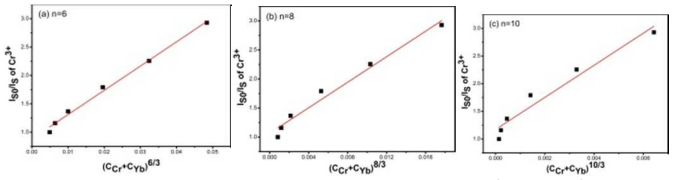

Figure 6. Dependence of I_{S0}/I_S of Cr^{3+} on (a) $C^{6/3}$ (b) $C^{8/3}$ and (c) $C^{10/3}$

On the basis of Dexter's energy transfer formula of multipolar interaction and Reisfeld's approximation the following relation can be obtained by[31, 32]

$$\frac{\eta_0}{\eta}\propto C^{n/3} \quad (3)$$

Where η_0 and η are, respectively, the luminescence quantum efficiency of Cr^{3+} in the absence and presence of Yb^{3+}; C is the sum of the content of Cr^{3+} and Yb^{3+}; n = 6, 8, and 10, corresponding to dipole -dipole, dipole-quadrupole, and quadrupole-quadrupole interactions, respectively. The value η_0/η is approximately calculated by the ratio of related luminescence intensities as[31]

$$\frac{I_{S0}}{I_S}\propto C^{n/3} \quad (4)$$

, where I_{S0} is the intrinsic luminescence intensity of Cr^{3+} and I_S is the luminescence intensity of Cr^{3+} in the presence of the Yb^{3+}. The I_{S0}/I_S - $C^{n/3}$ plot is represented in Figure 6a, b and c, and only when n = 6 does it show linear relation. This clearly indicates that the energy transfer from Cr^{3+} to Yb^{3+} is the dipole-dipole mechanism.

3.4 The photoluminescence enhancement by introduction of Gd^{3+}, Bi^{3+} and La^{3+}

This section writes on how we enhance the NIR emission intensity. The concentration of Yb^{3+} and Cr^{3+} are both kept at 7% which thought to be the best concentration. The dependence of the integrated NIR emission intensity of 983 nm under excitation of 420 nm radiation on the M^{3+} (M= Lu, Gd, Bi, La) doped $Y_{0.93}Yb_{0.07}Al_{2.79}Cr_{0.21}(BO_3)_4$ phosphors is shown in Figure 7. As the Gd^{3+} doping concentration increases, the NIR emitting intensity from Yb^{3+} first increases, reaching a maximum value when the Gd^{3+}concentration is equal to that of Yb^{3+} (7%). Then it decreases, accompanying a further increase of Gd^{3+} concentration(Figure 7a). It happened when replace Y^{3+} with Bi^{3+} (Figure 7b) and La^{3+} (Figure 7c), coming to maximum value when the concentration are 9% and 7%, respectively. We also substituted Lu^{3+} for Y^{3+}, found that NIR emitting intensity didn't increase but decrease (date not shown).

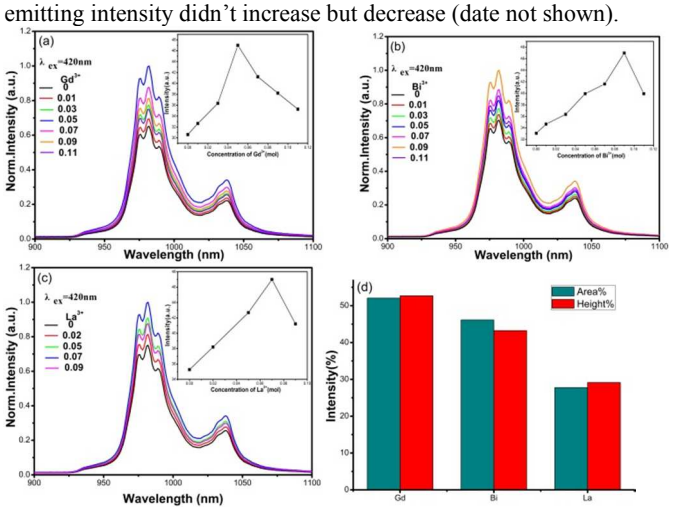

Figure 7. Normalized PL spectra for (a)$Y_{0.93-x}Gd_xYb_{0.07}Al_{2.79}Cr_{0.21}(BO_3)_4$ (b) $Y_{0.93-x}Bi_xYb_{0.07}Al_{2.79}Cr_{0.21}(BO_3)_4$ (c) $Y_{0.93-x}La_xYb_{0.07}Al_{2.79}Cr_{0.21}(BO_3)_4$ in near infrared area (excited at 420nm).(d) the comparison of relative intensity with different cations.

The Ionic Radii (Å) of cations for CN=6 are shown in Table 4. The size order of ionic radius is $Lu^{3+} < Y^{3+} < Gd^{3+} < Bi^{3+} < La^{3+}$. We can draw such a conclusion when the substituendum's Radii is less than Y^{3+}, it was useless for improving the emission intensity, but when the substituendum's Radii is greater than Y^{3+}, the emission intensity would strengthen effectively. This means that the replacement of Y^{3+} with Gd^{3+}, Bi^{3+}, and La^{3+} will result in better emission intensities of Yb^{3+}.

Table 4. Ionic Radii (Å) for CN=6

Ion	Radii(Å)	Ion	Radii(Å)	Ion	Radii(Å)
Y^{3+}	0.9	Al^{3+}	0.535	Gd^{3+}	0.938
Yb^{3+}	0.868	Cr^{3+}	0.615	Bi^{3+}	1.03
Nd^{3+}	0.983	Lu^{3+}	0.861	La^{3+}	1.032

And we compared the relative emission intensity of different cations to $Y_{0.93}Yb_{0.07}Al_{2.79}Cr_{0.21}(BO_3)_4$ in different aspects, relative integral area of discharge and relative height, the results are shown in the form of a histogram in figure 7d. Both of the two aspects show that when the substitute ionic radius exceeds Y^{3+}, the closer the radius to Y^{3+}, the better emission intensity we will get. Theoretical reasons for this phenomenon will be studied in our next researches.

3.5 Broaden $YAl_3(BO_3)_4:Cr^{3+},Yb^{3+}$ NIR PL bandwidth by introduction of Nd^{3+}

This section writes on how we broaden the NIR PL bandwidth. Cr^{3+}-Nd^{3+} co-doped YAB were first studied to establish the Nd^{3+} doping content. The concentration of the activator is kept at 7% for Cr^{3+}, and that of Nd^{3+} concentration is changed from 0 to 15%. Figure 8a shows the PL and PLE spectra for eight Cr^{3+} and Nd^{3+} -coactivated $Y_{1-m}Nd_mAl_{2.71}Cr_{0.21}(BO_3)_4$ phosphors with different dopant contents m of 0, 0.01, 0.03, 0.05, 0.07, 0.09, 0.13 and 0.15, respectively. They showed the same trend to $Y_{1-n}Yb_nAl_{2.71}Cr_{0.21}(BO_3)_4$ phosphors. Figure 8b plots the NIR emission spectra of the samples with different Nd^{3+} concentration, the near-infrared emission originated from Nd^{3+}: $^4F_{9/2}\rightarrow{}^4I_{11/2}$ transition can also be clearly observed under the excitations of Cr^{3+}: $^4T_1$ and $^4T_2$ energy levels, which indicates the energy transfer from Cr^{3+} to Nd^{3+}. Under 420 nm excitation, with increasing Nd^{3+} concentration, the emission intensity of Cr^{3+} decreases and the emission intensity of Nd^{3+} increases, maximizing at about n= 0.09. Concentration quenching occurs when n is higher than 0.07.

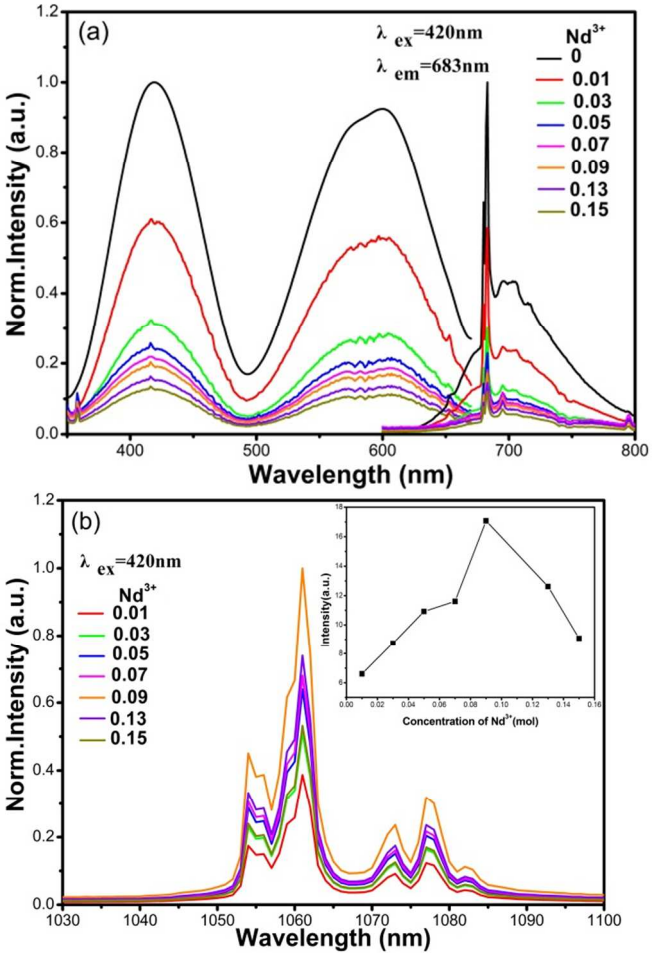

Figure 8. (a) Normalized excitation and emission spectra of $Y_{1-m}Nd_mAl_{2.71}Cr_{0.21}(BO_3)_4$. (b) Normalized emission spectra of $Y_{1-m}Nd_mAl_{2.71}Cr_{0.21}(BO_3)_4$ at the NIR region

Then we chose the both best doping amount of Yb^{3+} and Nd^{3+}, the concentration of the activator Cr^{3+} is also kept at 7%. Cr^{3+}, Yb^{3+}, Nd^{3+}-tri-doped YAB was synthesized. Figure 8b shows the NIR PL spectra of $Y_{0.86}Nd_{0.07}Yb_{0.07}Al_{2.71}Cr_{0.21}(BO_3)_4$. The near-infrared emission originated from Yb^{3+}: $^2F_{5/2}\rightarrow{}^2F_{7/2}$ and Nd^{3+}: $^4F_{9/2}\rightarrow{}^4I_{11/2}$ transition can be clearly observed under the excitations of Cr^{3+}: $^4T_1$ and $^4T_2$ energy levels (red line in Figure 9(a)), which indicates the energy transfer occurs from Cr^{3+} to Yb^{3+} and Nd^{3+}.According to Figure 9(a), the NIR PL bandwidth is explained by means of the tri-doped method.

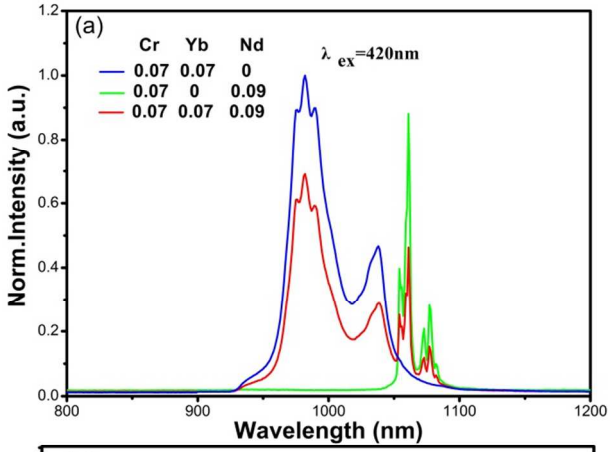

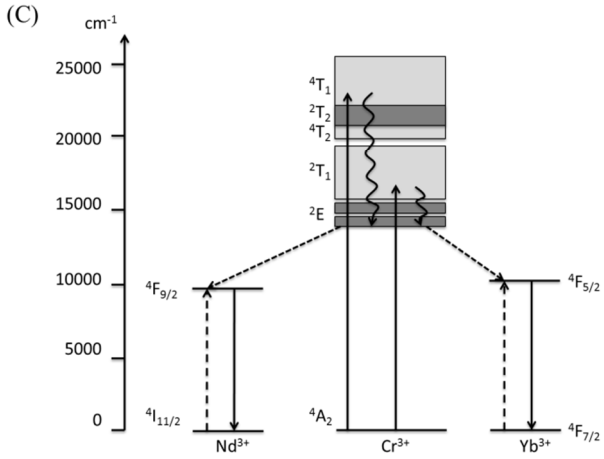

Figure 9. (a) Normalized emission spectra of $Y_{0.86}Nd_{0.07}Yb_{0.07}Al_{2.71}Cr_{0.21}(BO_3)_4$ at the NIR region. (b) Photoluminescence decay curves of Cr^{3+} in different doping cations (c) the energy level diagram of Cr^{3+}, Yb^{3+} and Nd^{3+} ions in $YAl_3(BO_3)_4$

Figure 9(b) displays the Photoluminescence decay curves of Cr^{3+} in $YAl_{2.71}Cr_{0.21}(BO_3)_4$, $Y_{0.93}Yb_{0.07}Al_{2.71}Cr_{0.21}(BO_3)_4$, $Y_{0.93}Nd_{0.07}Al_{2.71}Cr_{0.21}(BO_3)_4$ and $Y_{0.86}Nd_{0.07}Yb_{0.07}Al_{2.71}Cr_{0.21}(BO_3)_4$ phosphors, on the basis of eq 1 and decay curves, the lifetime values were determined to be 158.39, 76.94, 46.57 and 39.74μs, respectively. The decrease of lifetime values indicates that energy transfer occurs in both Cr^{3+} to Yb^{3+} and Cr^{3+} to Nd^{3+}. The energy level diagram of Cr^{3+}, Yb^{3+} and Nd^{3+} ions in $YAl_3(BO_3)_4$ is shown in figure 9 (c).

In order to check the influence of the phosphors on c-Si solar cell, we have built a solar cell device equipped with a luminescent solar concentrator. The schematic image of this device is shown in fig. 10 (a). The solar concentrator consists of a flat transparent slab covering luminescent down-shifting phosphors YAB:Cr^{3+},Yb^{3+}. The luminescent material absorbs incoming solar light and re-emits it at a longer wavelength isotropically. The emitted light, trapped in the slab via total internal reflection, is then guided to solar cells placed next to the edge of the slab.[33, 34]

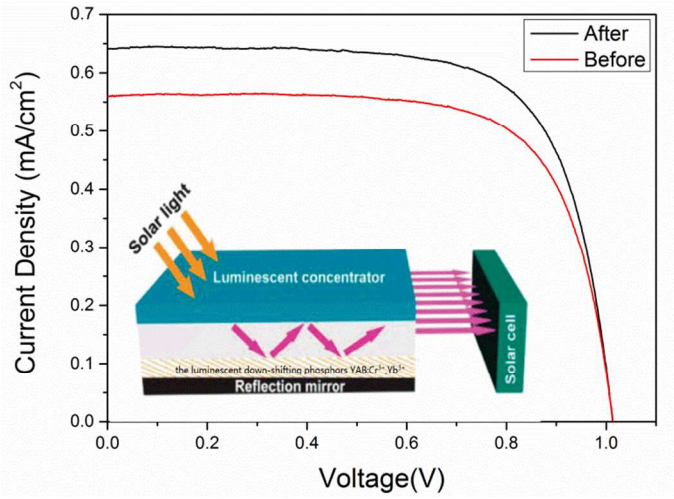

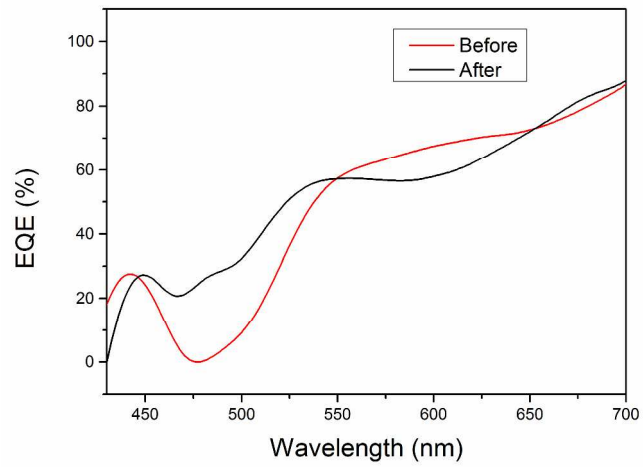

Figure 10 (a) *J-V* characteristics and (b) EQE as function of the wavelength for the c-Si solar cell before and after employing the down-shifting phosphor YAB:Cr^{3+},Yb^{3+}. Insert is The schematic image of a solar cell device equipped with a luminescent solar concentrator

The performances of c-Si Solar cells are characterized by the *J-V* curves under the condition of AM1.5 illumination, as shown in figure 10 (a). After employing the down-shifting phosphor YAB:Cr^{3+},Yb^{3+}, the short-circuit current density (J_{sc}) is enhanced 14.3%, compared to the reference c-Si solar cell before employing the phosphor. The short-circuit current density is proportional to the conversion efficiency from incident photons to electrical current.

The reason for the enhanced short-circuit current density may be found in the EQE spectra. In figure 10 (b), the red curve states that the bare commercial c-Si Solar cell shows very poor spectral response in the blue region. While, after the down-shifting phosphor is employed, YAB:Cr^{3+},Yb^{3+} converts high energetic photons (<500nm) into low energetic ones (namely around 1000 nm) which are transferred into the silicon solar cell. Consequently, according to the black curve in figure 10 (b), the spectral response in the blue-green region is obviously enhanced. We have to admit that the spectral response in the red region decreases because some useful red photons for this commercial Si solar cell are also transformed by the YAB:Cr^{3+},Yb^{3+} phosphor. But, we believe this problem may be solved by choosing appropriate Si solar cell whose response spectrum matches better with the converting phosphors.

4 Conclusion

Broadband excitation and strong NIR emission Cr^{3+} spectra converts $Y_{1-n}Yb_nAl_{2.79}Cr_{0.21}(BO_3)_4$, $Y_{1-m}Nd_mAl_{2.79}Cr_{0.21}(BO_3)_4$ and $Y_{0.86}Yb_{0.07}Nd_{0.07}Al_{2.79}Cr_{0.21}(BO_3)_4$ were prepared. In all the above solid solution phases sensitizer Cr^{3+} ions occupy Al^{3+} sites in the $YAl_3(BO_3)_4$ lattice. The absorption of $YAl_3(BO_3)_4$:Cr^{3+} spans the spectral range of 370 – 750 nm. This enables broadband sensitization of Yb^{3+}. Energy transfer occurs from Cr^{3+}: $^4T_2$ to Yb^{3+}: $^2F_{5/2}$. The occurrence of this energy process is evidenced by reduced red PL from Cr^{3+}, reduced corresponding PL lifetime and reduced external quantum efficiency with increasing Yb^{3+} concentration, and identical PLE spectra for monitoring PL from Cr^{3+} and NIR PL from Yb^{3+}. The Dexter's energy transfer formula of multipolar interaction and Reisfeld's approximation model applied to the analysis of the decay curves has indicated the dipole–dipole interaction mechanism as mainly responsible for the transfer. The replacement of Y^{3+} with Gd^{3+}, Bi^{3+}, and La^{3+} could result in the better emission intensities of Yb^{3+}. Also the introduction of Nd^{3+} acquires wider PL emission bandwidth. As the Cr^{3+} has not only broadband absorption in the visible region but also high pump efficiency, the Cr^{3+}-Yb^{3+}/Nd^{3+} doped YABs are expected to be developed as spectral convertors for silicon solar cells to enhance the photovoltaic conversion efficiency.

Acknowledgements

This work is supported by Shanghai Science & Technology Committee (12521102501), Shanghai Educational Committee (11ZR1426500), Innovation Program of Shanghai Municipal Education Commission (14ZZ127), PCSIRT(IRT1269), and the Program of Shanghai Normal University (DZL124)

Notes and references

a The Education Ministry Key Laboratory of Resource Chemistry and Shanghai Key Laboratory of Rare Earth Functional Materials, Department of Chemistry, Shanghai Normal University, Shanghai 200234, People's Republic of China

b Foreign Languages and Applied Linguistic, School of Foreign Languages, East China Normal University, Shanghai 200234, People's Republic of China

Electronic Supplementary Information (ESI) available: [details of any supplementary information available should be included here]. See DOI: 10.1039/b000000x/

1. X. Huang, S. Han, W. Huang and X. Liu, *Chem Soc Rev*, 2013, 42, 173-201.
2. G. D. Scholes, G. R. Fleming, A. Olaya-Castro and R. van Grondelle, *Nature chemistry*, 2011, 3, 763-774.
3. O. Morton, *Nature*, 2006, 443, 19-22.
4. A. J. Nozik and J. Miller, *Chem. Rev.*, 2010, 110, 6443-6445.
5. B. S. Richards, *Sol. Energy Mater. Sol. Cells*, 2006, 90, 2329-2337.
6. B. M. van der Ende, L. Aarts and A. Meijerink, *Adv. Mater.*, 2009, 21, 3073-3077.
7. Y. Peng, J. Liu, K. Zhang, H. Luo, J. Li, B. Xu, L. Han, X. Li and X. Yu, *Appl. Phys. Lett.*, 2011, 99, 121110-121112.
8. L. Aarts, B. M. van der Ende and A. Meijerink, *J. Appl. Phys.*, 2009, 106, 023522-.
9. D. C. Yu, X. Y. Huang, S. Ye and Q. Y. Zhang, *J. Alloys Compd.*, 2011, 509, 9919-9923.
10. Q. Y. Zhang, C. H. Yang, Z. H. Jiang and X. H. Ji, *Appl. Phys. Lett.*, 2007, 90, 061914.
11. W. Zheng, H. Zhu, R. Li, D. Tu, Y. Liu, W. Luo and X. Chen, *Phys Chem Chem Phys*, 2012, DOI: 10.1039/c2cp24044k, 6974-6980.
12. J. Zhou, Y. Teng, S. Ye, Y. Zhuang and J. Qiu, *Chem. Phys. Lett.*, 2010, 486, 116-118.
13. J. Zhou, Y. Zhuang, S. Ye, Y. Teng, G. Lin, B. Zhu, J. Xie and J. Qiu, *Appl. Phys. Lett.*, 2009, 95, 141101-141103.
14. Y. Teng, J. Zhou, X. Liu, S. Ye and J. Qiu, *Opt. Express*, 2010, 18, 9671-9676.
15. X. Y. Huang, J. X. Wang, D. C. Yu, S. Ye, Q. Y. Zhang and X. W. Sun, *Journal of Applied Physics*, 2011, 109, 113526.
16. B. C. Rowan, L. R. Wilson and B. S. Richards, *IEEE Journal of Selected Topics in Quantum Electronics*, 2008, 14, 1312-1322.
17. S. M. Borisov, K. Gatterer, B. Bitschnau and I. Klimant, *J. Phys. Chem. C*, 2010, 114, 9118-9124.
18. Z. LIU and Y. SEGAWA, *Jpn. J. Appl. Phys*, 1995, 34, 2338-2343.
19. T.-C. Liu, G. Zhang, X. Qiao, J. Wang, H. J. Seo, D.-P. Tsai and R.-S. Liu, *Inorg. Chem.*, 2013, 52, 7352–7357.
20. S. Sivakumar, F. C. M. van Veggel and P. S. May, *J. Am. Chem. Soc.*, 2007, 129, 620-625.
21. C. Lin, R. Liu, Y. Tang and S. Hu, *J. Electrochem. Soc.*, 2008, 155, J248-J251.
22. G. Wang, H. Gallagher, T. Han and B. Henderson, *J. Cryst. Growth*, 1996, 163, 272-278.
23. M. Yamaga, Y. Oda, H. Uno, K. Hasegawa, H. Ito and

S. Mizuno, *J. Appl. Phys.*, 2012, 112, 063508-063508.
24. I. Nikolov, X. Mateos, F. Güell, J. Massons, V. Nikolov, P. Peshev and F. Dıaz, *Opt. Mater.*, 2004, 25, 53-58.
25. H. Szymczak, M. Wardzynska and I. Mylnikova, *Journal of Physics C: Solid State Physics*, 1975, 8, 3937.
26. X. Huang, J. Wang, D. Yu, S. Ye, Q. Zhang and X. Sun, *J. Appl. Phys.*, 2011, 109, 113526-113526.
27. X. Wei, S. Huang, Y. Chen, C. Guo, M. Yin and W. Xu, *J. Appl. Phys.*, 2010, 107, 103107.
28. H. Luo, J. Liu, X. Zheng, L. Han, K. Ren and X. Yu, *J. Mater. Chem.*, 2012, 22, 15887.
29. Z. Xia and R.-S. Liu, *J. Phys. Chem. C*, 2012, 116, 15604-15609.
30. G. Blasse and B. Grabmaier, *Luminescent materials*, Springer-Verlag Berlin, 1994.
31. P. I. Paulose, G. Jose and N. V. Unnikrishnan, *J. Non-Cryst. Solids*, 2010, 356, 93-97.
32. R. Reisfeld and N. Lieblich-Soffer, *J. Solid State Chem.*, 1979, 28, 391-395.
33. M. G. Debije and P. P. C. Verbunt, *Advanced Energy Materials*, 2012, 2, 12-35.
34. D. K. G. de Boer, D. J. Broer, M. G. Debije, W. Keur, A. Meijerink, C. R. Ronda and P. P. C. Verbunt, *Opt. Express*, 2012, 20, A395-A405.

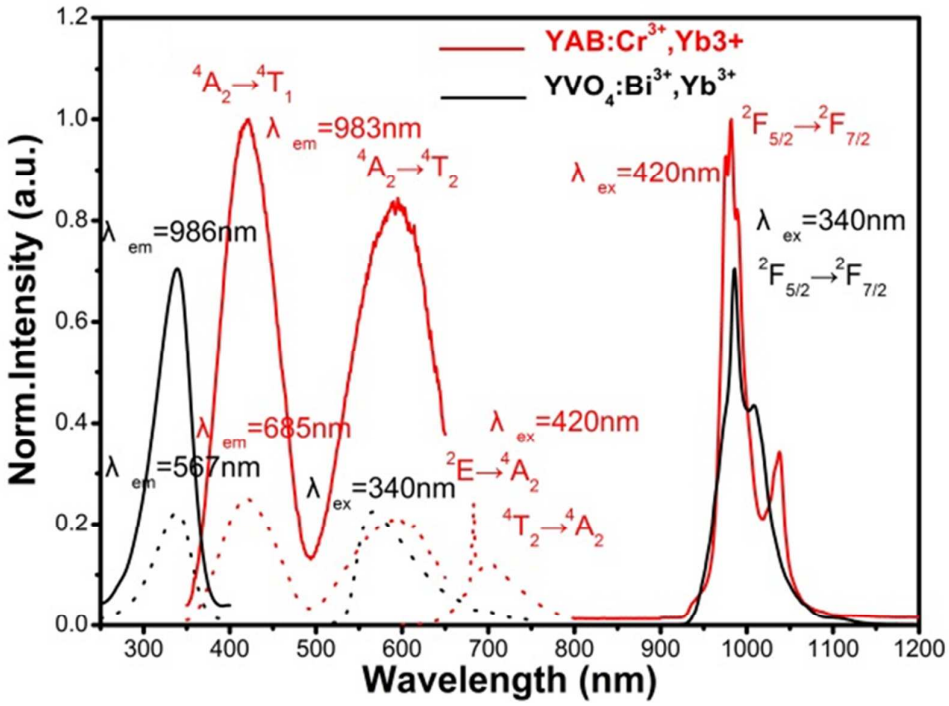

By taking advantage of the spin allowed $^4A_2 \rightarrow {}^4T_2$ and $^4A_2 \rightarrow {}^4T_1$ absorption of Cr^{3+} and the efficient energy transfer to Yb^{3+}. The Cr^{3+}-Yb^{3+} co-doped YAB could convert almost high-energy UV-Vis photons into low-energy NIR photons efficiently, which benefit the enhancement of silicon solar photovoltaic conversion efficiency.